THE JOURNAL OF PHYSICAL CHEMISTRY C

Article

Cite This: J. Phys. Chem. C 2019, 123, 27207−27213

pubs.acs.org/JPCC

Ultrafast Charge Carrier Dynamics and Nonlinear Optical Absorption of InP/ZnS Core−Shell Colloidal Quantum Dots

Bowen Zhang,[†] Xinwei Wang,*[,†,‡] Dengkui Wang,[†] Jilong Tang,[†] Xuan Fang,[†] Dan Fang,[†] Xiaohua Wang,*[,†] Rui Chen,*[,§] Tingchao He,[∥] and Zhipeng Wei[†]

[†]State Key Laboratory of High Power Semiconductor Laser, School of Science, and [‡]School of Materials Science and Engineering, Changchun University of Science and Technology, 7089 Wei-Xing Road, Changchun 130022, China

[§]Department of Electrical and Electronic Engineering, Southern University of Science and Technology, Shenzhen, Guangdong 518055, China

[∥]College of Physics and Optoelectronic Engineering, Shenzhen University, Shenzhen 518060, China

Supporting Information

ABSTRACT: Understanding of ultrafast carrier dynamics in InP/ZnS colloidal quantum dots (QDs) is essential for their optoelectronic applications. In this paper, we have successfully fabricated high-quality InP/ZnS core−shell QDs with quantum yield (QY) of 47%. Time-resolved photoluminescence (TRPL) and femtosecond transient absorption (TAS) measurements were performed to characterize the carrier injection, relaxation, and transition process in the InP/ZnS QDs. It is found that the photoexcited carrier first injected to the ZnS shell in 2 ps, then relaxed to the alloyed layer between the ZnS shell and InP core in 7.4 ps, next relaxed to different energy levels in the InP core in about 170 ps, and finally recombined by charged and neutral excitons transition in 4.1 and 26.7 ns, respectively. Additionally, the two-photon absorption (TPA) coefficient obtained from Z-scan measurement indicates that InP/ZnS QDs possess good nonlinearly optical properties. Our research is significant for the improvement and engineering of InP/ZnS QDs-based materials for optoelectronic applications.

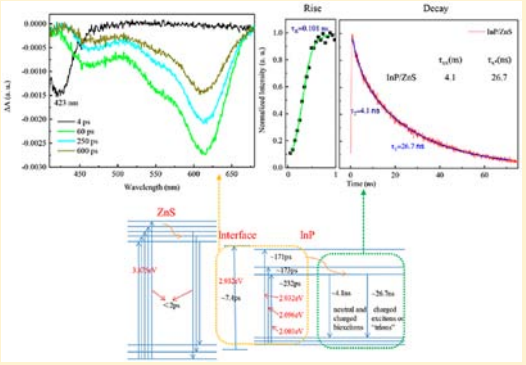

1. INTRODUCTION

Colloidal quantum dots (QDs) are a new class of materials developed in the past several decades which show attractive applications related to light emission and absorption,[1−3] such as light-emitting devices,[4,5] photodetection,[6] and solar energy conversion.[7] So far, there have been a lot of literatures reporting on the InP-based QDs due to their good photostability, broader tunable emission, and potential application in the nonlinearly optical area.[8,9] Among them, the core−shell structure QDs exhibit a higher emission quantum yield (QY) due to the reduced nonradiative recombination centers by the surface passivation of $ZnCdSe_2$, ZnS, and so on.[10,11] So far, most researchers have focused on the synthesis and optical properties investigation of InP-based QDs. For example, to enhance the emission and QY of InP QDs, Micic and co-workers have modified the surface of the InP particle by using HF or epitaxially grown a shell of wider band gap semiconductors $ZnCdSe_2$[12−14] based on initial synthetic approaches.[15] Peng has realized industrial mass production through the effective regulation of reaction parameters and the selection of effective reagents, such as ODE or octaamine.[16,17] Recently, Yang and co-workers reported a novel synthesis method to facilitate the production of InP and InP/ZnS NCs, which has stimulated intensive optical studies due to the easier fabrication of high quality materials.[18,19] In addition, the steady-state optical performance of InP/ZnS quantum dots has been studied in detail by temperature- and power-dependent photoluminescence (PL) measurements.[20−22] Previous research about the steady-state PL properties measurement of hydrofluoric acid (HF) etched colloidal InP NCs by Micic et al.[12] showed that the emission comes from a spin-forbidden dark exciton state at low temperature. More recent work by Biadala studied luminescence of InP/ZnS and analyzed the fine structure of the band edge emission, which is considered to include two sources of luminescent centers, namely the optical excitons and the optically inhibited states.[23] However, to the best of our knowledge, only a few studies have addressed the ultrafast carrier dynamics of semiconductor QDs,[24] especially the InP/ZnS QDs, which is indispensable to understand carrier injection and transition process for better optoelectronic applications. Hence, it is very important to study the ultrafast dynamic process in InP/ZnS QDs.

Herein, we have synthesized high-quality InP/ZnS core−shell QDs with QY of 47% via a one-pot method. InP/ZnS has

Received: July 25, 2019
Revised: September 11, 2019
Published: October 14, 2019

DOI: 10.1021/acs.jpcc.9b07092
J. Phys. Chem. C 2019, 123, 27207−27213

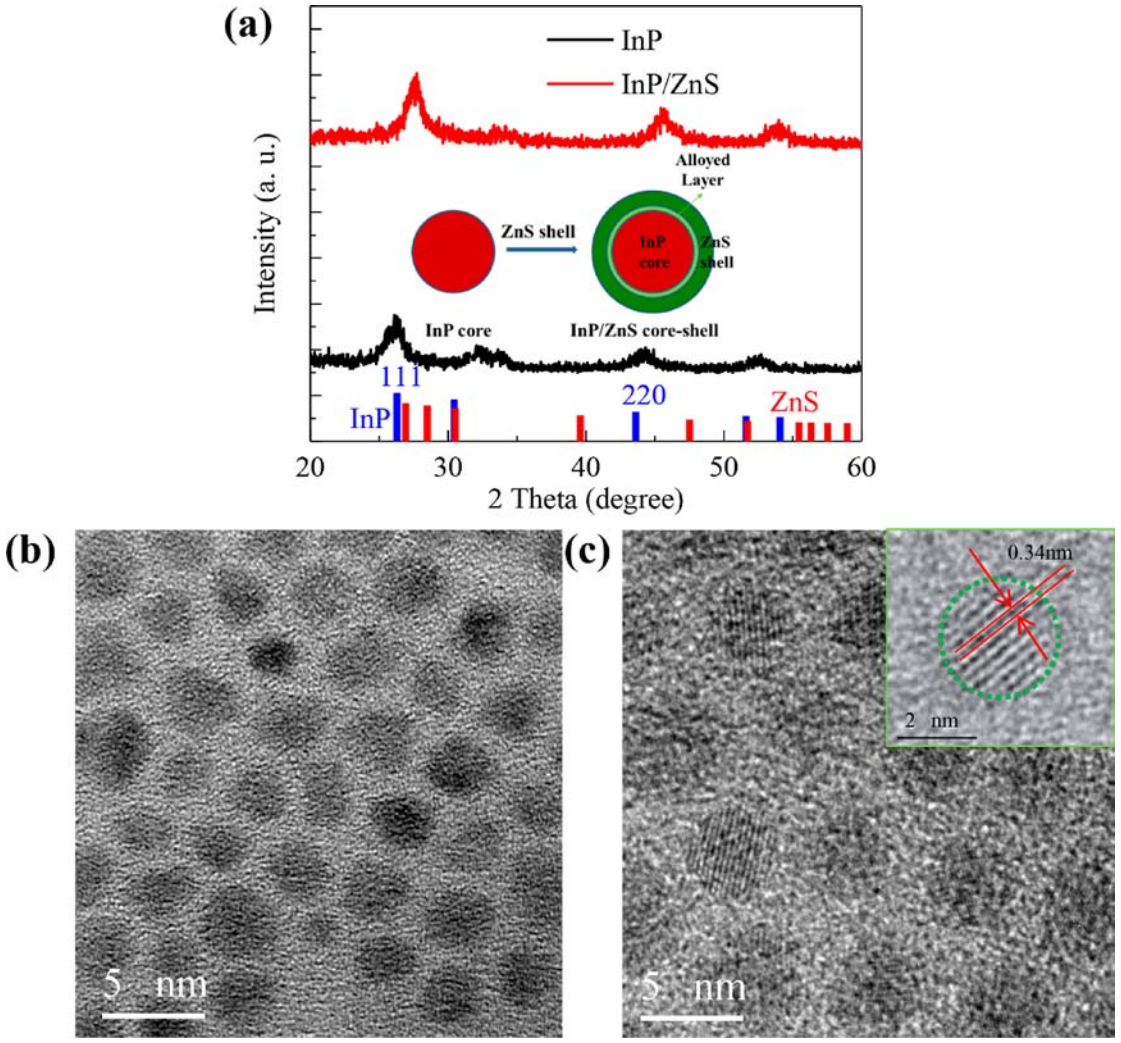

Figure 1. (a) Powder X-ray diffraction patterns of the InP and InP/ZnS QDs; the inset is the schematic illustration of both types of QDs. (b) TEM images of InP QDs. (c) HRTEM images of InP/ZnS QDs; the inset is the HRTEM images of single InP/ZnS QDs.

a typical type I band structure, the energy band of ZnS is much larger than that of InP, and the carrier recombination is confined to the InP core. Ultrafast carrier dynamics of carrier injection and transition inside InP/ZnS QDs were investigated by ultrafast transient absorption spectroscopy (TAS) and time-resolved photoluminescence (TRPL) measurements. The TAS measurement reveals the injection and relaxation processes of photoexcited carrier over time in InP/ZnS QDs. It shows that the photogenerated carrier was first injected to the ZnS shell within 2 ps, then relaxed to the alloyed layer between the ZnS shell and InP core in 7.4 ps, and next transitioned to different energy levels in the InP core in about 170 ps. The lifetimes of charged and neutral excitons transition of InP/ZnS QDs were determined to be 4.1 and 26.7 ns, respectively, by TRPL. Additionally, the two-photon absorption coefficient derived from Z-scan technology indicates that InP/ZnS QDs possess good nonlinear optical properties.

2. EXPERIMENTAL DETAILS

Materials. Indium(III) chloride ($InCl_3$, 99.999%), Zn chloride ($ZnCl_2$, 98%), tris(dimethylamino)phosphine (P(N-$(CH_3)_2)_3$, 97%), Zn stearate (10−12% Zn basis), 1-octadecene (ODE,90%), 1-dodecanethiol (DDT, 98%), oleylamine (OLA, 70%), and solvents were purchased from Sigma-Aldrich.

Synthesis of InP and InP/ZnS Core/Shell QDs. InP/ZnS nanocrystals were synthesized based on protocols published on other papers.[18,19] Indium(III) chloride (200 mg, 0.45 mmol) and zinc(II) chloride (122 mg, 2.2 mmol) were mixed with the coordinating solvent dodecylamine (3 mL). The mixture was stirred at 200 °C under an inert atmosphere for 1 h and then cooled to 180 °C. Then 0.25 mL of tris(dimethylamino)phosphine was quickly injected into the above mixture. After the injection of phosphorus precursor, the InP nanocrystals' synthesis proceeded. The InP core reaction occurred for 5 min. At 5 min: slow injection of 0.7 mL of saturated TOP-S (2.2 M). At 8 min: temperature increased from 180 to 240 °C. At 60 min: slow injection of 1 g of $Zn(stearate)_2$ in 4 mL of octadecene. (From this step, the growth of the ZnS shell begins, and further core growth can be ruled out due to the decrease of the In and P precursor's concentration and the rise of the temperature.) At 90 min: injection stoichiometric TOP-S (2.2 M) of 0.7 mL. At 210 min: injection of 1 g of $Zn(stearate)_2$ in 4 mL of octadecene. At 225 min: slow injection of 0.7 mL of stoichiometric TOP-S (2.2 M). At 290 min: end of reaction. The temperature cooled when the reaction stopped. Then, the InP/ZnS nanocrystals were precipitated in ethanol and suspended in chloroform. The

DOI: 10.1021/acs.jpcc.9b07092
J. Phys. Chem. C 2019, 123, 27207−27213

InP core diameter was 3.1 nm, and a 1.1 nm thick ZnS shell was prepared.

Characterization. PL QYs of the samples were obtained by comparing their integrated emission intensity with the R6G dye molecule in ethanol (QY of ~96%) with an optical density of ~0.05. During the measurement, a 442 nm He−Cd laser was used as the excitation source. High-resolution transmission electron microscopy (TEM) images of the QDs were characterized by a JEOL JEM-4010 electron microscope operated at an accelerating voltage of 400 kV. X-ray diffraction (XRD) (Bruker, D8 Focus) using Cu Ka radiation was utilized to characterize the crystal structure and average size of QDs.

The ultrafast carrier dynamics of the samples were characterized by the ultrafast pump−probe transient absorption system. The femtosecond laser has a central wavelength of 800 nm with a pulse width of 100 fs and a repetition rate of 1 kHz. The 400 nm pump laser was generated by the frequency multiplication of the BBO crystal with a 800 nm laser. The probe pulses were white light with a wavelength of 320−800 nm and generated from a thin CaF_2 plate under the excitation of a 800 nm laser. The changes in absorbance were measured between every two successive laser shots by chopping the pump beam at 500 Hz. The light jitter was eliminated by using two silicon-based detectors to compare the individual probe light with the probe light in the pump sample. The spot sizes of pump and probe on the sample are 280 and 180 μm, which were determined by the knife edge method.

The TRPL were taken by a compact luminescent lifetime spectrometer (C11367, Hamamatsu) with a C11367-11 photomultiplier tube. The wavelength of the excitation was 400 nm with a repetition rate of 1 MHz. The nonlinear optical property measurements were taken by a homemade Z-scan system.[25] The excitation source was a femtosecond laser with a central wavelength of 800 nm with a pulse width of 100 fs and a repetition rate of 1 kHz. The excitation light was focused on the sample after passing through a focusing mirror with a focal length of 30 cm, and the sample was placed on a movable translation stage. The change in intensity of light transmitted through the sample was detected by a silicon photodetector.

3. RESULTS AND DISCUSSION

Figure 1a shows the powder X-ray diffraction (XRD) patterns of InP and InP/ZnS QDs. Both samples showed a zinc blende cubic crystal structure. Compared with InP QDs, after the coating of ZnS shell, the broadening diffraction peaks of InP/ZnS QDs shift obviously toward the positions between the InP and ZnS. This can be ascribed to the difference of lattice constant between InP and ZnS (lattice mismatch 7.7%) as described before.[26] At the same time, through the Raman spectrum of the InP/ZnS quantum dots (see the Supporting Information, Figure S1), it is inferred that the alloy interface is formed between the InP core and the ZnS shell due to interdiffusion. The subsequent transient absorption spectrum also verified this conclusion, and the diffraction peaks of InP/ZnS QDs become higher than InP QDs. The above results imply the formation of the core/shell structure with the remarkable crystal quality. The inset shows the schematic diagram of the InP core and InP/ZnS core−shell structure. Transmission electron microscopy (TEM) images of the samples are shown in Figure 1b to reveal the morphologies of the materials. It can be seen that the InP QDs are homogeneously sphere-like nanoparticles, with average size around 3.2 nm by calculating the mean value from arbitrary 200 QDs (Figure S2). The diameter of the QDs after ZnS shell coating increases to 5.4 nm by calculating the mean value from arbitrary 200 QDs (see Figure S2), indicating that a 1.1 nm shell has been grown; the shell layer includes an alloy interface and a separate ZnS layer. To clearly observe the crystal structure, the corresponding enlarged HRTEM image of the QDs shows that the interlayer lattice planes of the InP/ZnS QDs have a spacing about 0.34 nm (inset of Figure 1c), which is consistent with the (111) crystal plane of the sphalerite structure InP.[27,28]

Figure 2a shows the absorption spectrum (blue line) of InP QDs in toluene. Two excitonic features at about 480 and 550

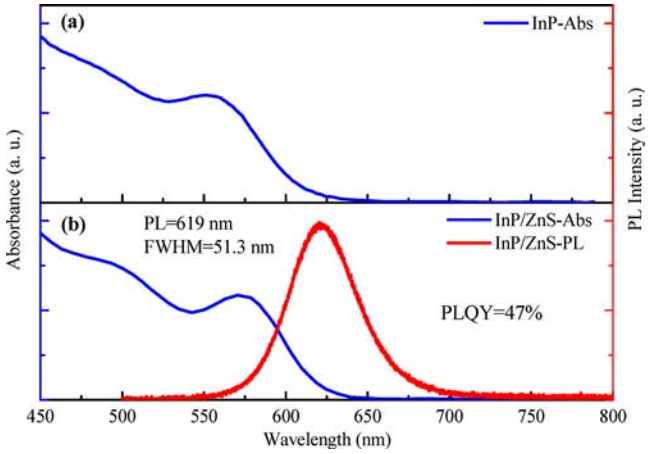

Figure 2. (a) Absorption spectra (blue line) of InP QDs. (b) PL spectra (red line) and absorption spectra (blue line) of InP/ZnS QDs.

nm separated by 0.33 eV can be observed. The two peaks can be ascribed to the optical transitions between two different energy levels, which is caused by the energy splitting. The energy difference between the two energy levels is consistent with the calculated result.[29] It should be pointed out that the as-grown InP core QDs does not show any emission. Figure 2b shows the absorption spectrum (blue line) and PL spectrum (red line) of InP/ZnS QDs in toluene. After ZnS coating, the absorption peak exhibits a pronounced red-shift of about 65 meV, indicating the formation of ZnS shell in the samples. In addition, a narrow and strong PL emission at 619 nm (1.995 eV) has been detected of InP/ZnS QDs in toluene, which indicates good passivation of the InP cores by ZnS shells. It is noted that the photoexcitation of InP/ZnS QDs leads to exciton emission with a line width of 51.3 nm (0.158 eV) and a PLQY of 47%, which are close to the best reported data in the literature and at a similar emission wavelength. The exciton bandgap (in eV) can be calculated by the following equation according to the effective mass model for QDs with a Coulomb interaction.[30]

$$E_{g,QD} = E_{g,bulk} + \Delta E$$

$$\Delta E = \frac{\hbar^2\pi^2}{2er^2}\left(\frac{1}{m_e^*} + \frac{1}{m_h^*}\right) - \frac{1.786e}{4\pi\varepsilon\varepsilon_0 r}$$

where $E_{g,bulk}$ is the band gap of the bulk crystal, ΔE is the blue-shift caused by the quantum confinement effect, $\hbar = h/2\pi$ is the reduced Planck constant, e is the electron charge, $m_{e(h)}^*$ is the effective mass of electron (hole) in the bulk crystal, ε is the relative dielectric constant of the bulk crystal, and ε_0 is the

DOI: 10.1021/acs.jpcc.9b07092
J. Phys. Chem. C 2019, 123, 27207−27213

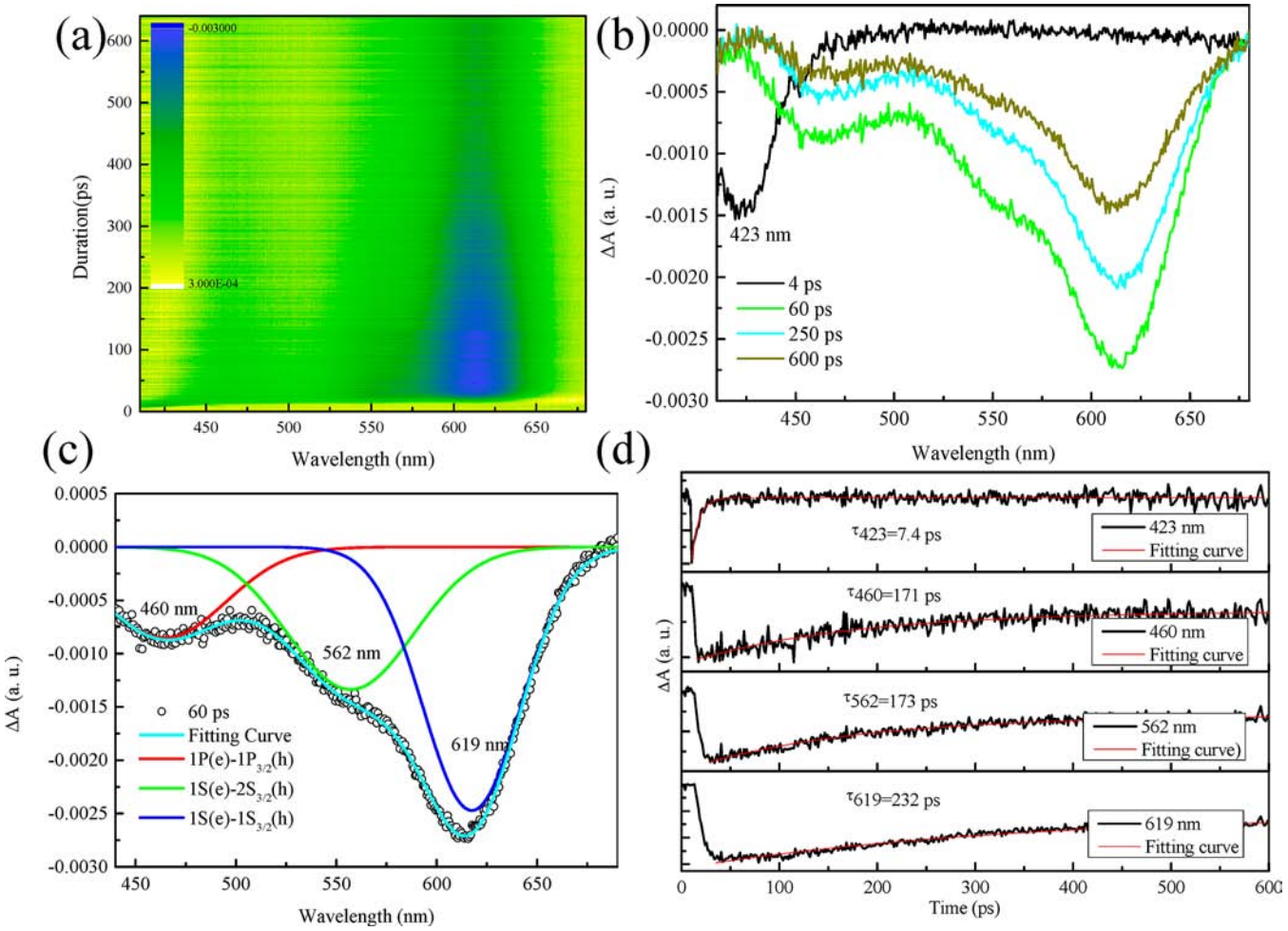

Figure 3. (a) Transient absorption spectra of InP/ZnS QDs. (b) Absorption spectra at different times after excitation. (c) Peak fitting of the spectrum after 60 ps. (d) Lifetime fitting curves at 423, 460, 562, and 619 nm.

permittivity. As the $E_{g,QD}$ of InP is 1.995 eV, we can conclude the size of InP is about 3.2 nm, the same as the valuable of TEM image.

To clearly understand the ultrafast carrier dynamics of InP/ZnS QDs, ultrafast transient absorption spectroscopy (TAS) was performed at room temperature. TAS provides the understanding of the carriers' dynamics occurring on picosecond (ps) time scales. Figure 3a shows the TAS of InP/ZnS QDs that exhibit four distinctive spectral features at 423, 460, 562, and 619 nm. There still is an absorption located at 320−380 nm with a lifetime of 7 ps (as shown in Figure S3), which aligned well with the band gap of ZnS. According to previous research in other core−shell QDs,[31,32] we assigned these processes to the surface state related carrier dynamics of the entire quantum dot. We have confirmed their origin using the analytical methods reported in previous Cd-based core−shell QDs literature.[33−36] For a further study of the spectra, we extracted the absorption spectra at different times (4, 60, 250, and 600 ps) after excitation (as shown in Figure 3b). According to the change over time, we conclude that there are two series origin of absorption: one located at 423 nm and other located at 450−650 nm. The absorption peak at 423 nm corresponds to the carrier transition in the alloyed layer between InP and ZnS. We then analyzed the absorption spectrum at 60 ps that was well-fitted by three peaks, corresponding to $1S(e)-1S_{2/3}(h)$, $1S(e)-2S_{2/3}(h)$, and $1P(e)-1P_{2/3}(h)$ transitions in the InP band at 619, 562, and 460 nm, respectively,[37,38] as shown in Figure 3c. The absorption of the four positions was fitted by time, as shown in Figure 3d, and the lifetimes at 423, 460, 562, and 619 nm can be obtained to be 7.4, 171, 173, and 233 ps, respectively. The lifetime of absorptions at 460, 562, and 619 nm are of the same order of magnitude—2 orders of magnitude higher than the lifetime of absorption at 423 nm. The different magnitudes of lifetime agreed with the conclusion that the absorption at 423 nm originates from the alloyed layer and the absorptions at 460, 562, and 619 nm origin from InP.

To discuss the carrier dynamics of the core−shell InP−ZnS QDs, time-resolved PL (TRPL) measurements on dilute QD solutions dispersed in toluene were performed. TRPL measures the carrier recombination dynamics occurring on nanosecond time scales. During the transient lifetime measurement, femtosecond laser pulses with a wavelength of 400 nm and a pulse width of 80 fs were used for excitation. Figure 4a shows the rise and decay curves of InP/ZnS QDs with their fitting results at room temperature. The rise time is determined by fitting the rising process with the Boltzmann sigmoidal function

$$I(t) = B_2 + \frac{B_1 - B_2}{1 + e^{(t-t_s)/\tau_R}}$$

DOI: 10.1021/acs.jpcc.9b07092
J. Phys. Chem. C 2019, 123, 27207−27213

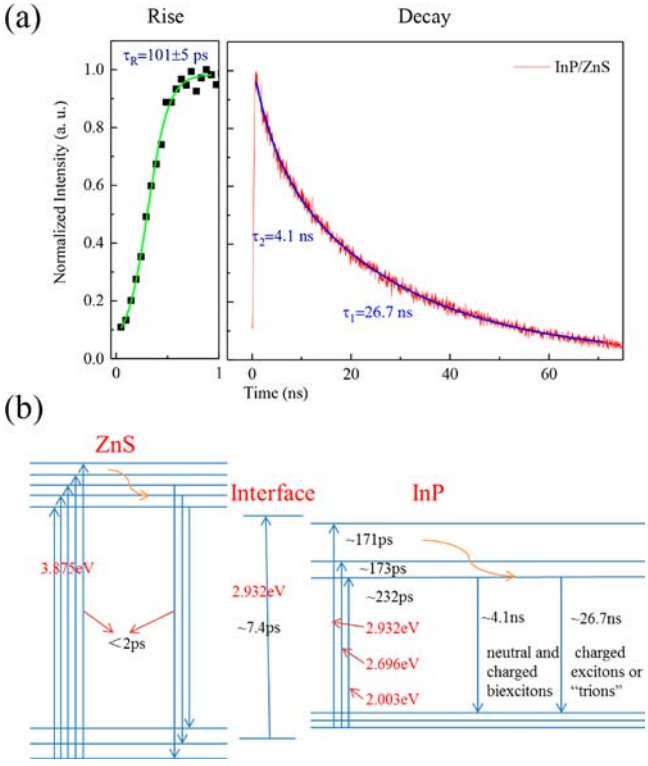

Figure 4. (a) Rise and decay curves of InP/ZnS QDs. The solid lines are the fitting curves. (b) Schematic illustration of carrier injection and transport in InP/ZnS QDs according to previous analyses.

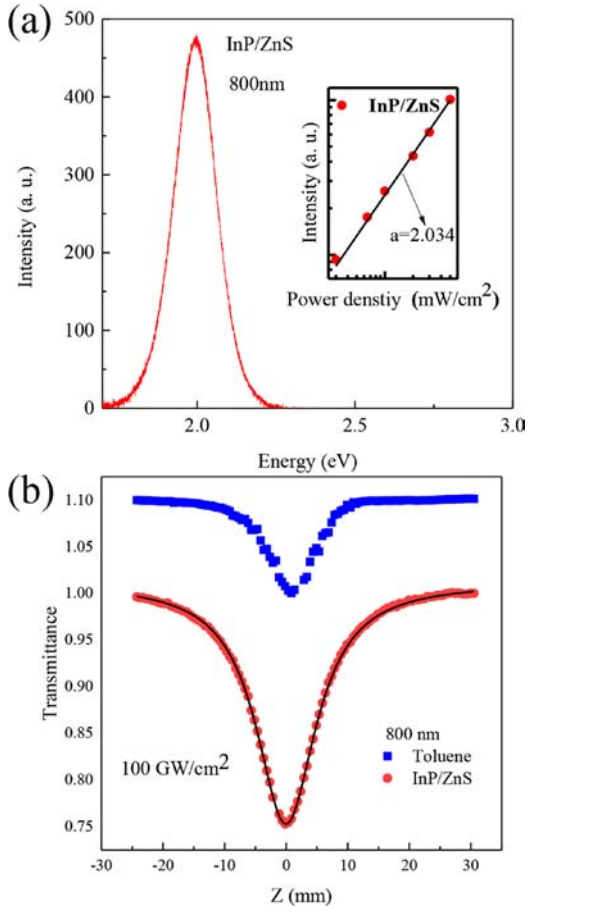

Figure 5. (a) PL spectra of the InP/ZnS QDs excited at 800 nm; the inset is the integrated intensity of emission with excitation power. (b) Open aperture Z-scan curves of InP/ZnS(C/S) QDs at the wavelength of 800 nm with input intensity of 100 GW/cm^2.

where B_1 is the initial value, B_2 is the final value, t_s indicates the time center, and τ_R represents the time constant for the rising process. The rise time (τ_R) for FX obtained from the fitting is 101 ± 5 ps (results shown in Figure 4a),[39] which value is larger than that in CdSe QDs (20−40 ps).[40,41] The decay curve of the QD samples can be well-fitted by a double-exponential function[38]

$$I(t) = A_1 e^{-t/\tau_1} + A_2 e^{-t/\tau_2} + I_b$$

where I_b represents the noise. The fitting results are plotted as solid lines in Figure 4a. The fitting parameters are τ_1 = 26.7 ns and τ_2 = 4.1 ns. On the basis of previous studies, we attribute the initial faster component to neutral and charged biexcitons, while the slower component to charged excitons or "trions".[32,42] According to the analysis of TAS and TRPL measurement, Figure 4b shows a schematic illustration of carrier injection and transportation in InP/ZnS QDs. The photoexcited carrier first injected to the ZnS shell in 2 ps, then relaxed to alloyed layer between ZnS shell and InP core in 7.4 ps, and next relaxed to different energy levels in the InP core in about 180 ps. After optical excitation, the electron and hole will undergo a fast thermalization process before the formation of an exciton and then relax to a K = 0 state before radiation. After relaxation or cooling, the charged excitons and neutral excitons recombined in 4.1 and 26.7 ns, respectively.

The exciton's Bohr radius of InP is about 15 nm, which theoretically suggests a good nonlinear optical property.[43] Here we tested the two-photon absorption coefficient of InP/ZnS QDs by the Z-scan technique. The inset of Figure 5a plots the log−log data of the integrated PL intensity with excitation power at 800 nm, where the solid lines are theoretical fitting by the equation $I = \eta I_0^{\alpha}$, and the fitting results of α is 2.034. The nearly quadratic intensity dependence of the emission proves the two-photon-induced emission rather than the Auger-type upconversion PL.[44] Figure 5a shows the two-photon excited PL of InP/ZnS QDs by 800 nm, which is similar to the one-photon excitation, and it indicates that the hot carriers under both one- and two-photon excitation relax to the same lowest energy level where the radiative recombination occurs. The open aperture Z-scan curves of InP/ZnS QDs in toluene at the same intensity are shown in Figure 5b. The open Z-scan curve of toluene is also shown to eliminate the effect of solvent, so that the change obtained from the measurement can be entirely ascribed to the QDs themselves. The normalized transmittance of InP/ZnS QDs can be well-fitted with the formula of TPA according to Z-scan theory.[25] The TPA coefficients for InP/ZnS QDs can be determined to be 0.0086 cm/GW. The TPA cross section σ_2 per InP/ZnS QD can be calculated according to the following formula:

$$\sigma_2 = \beta h\nu / N$$

where $h\nu$ is the photon energy and N is the particle concentration in the solution. Here, N is determined to be 5 × $10^{19}/l$, employing the empirical relationship between the first exciton absorption peak, molar extinction coefficient, and size.[45] The corresponding σ_2 are inferred to be 4.26 × 10^{-47} cm^4 s photon^{-1} (or 3.5 × 10^3 GM) for InP/ZnS QDs, which are comparable to or even larger than that of CdSe (5.1 × 10^3

DOI: 10.1021/acs.jpcc.9b07092
J. Phys. Chem. C 2019, 123, 27207−27213

GM), CdTe (2.1×10^3 GM), and CdS (4.4×10^3 GM) QDs at similar sizes.[46−48] The above results imply the synthesized InP/ZnS QDs possess an excellent nonlinear optical property.

4. CONCLUSIONS

The primary exciton dynamics of InP/ZnS core−shell QDs, including the carrier injection and transition process, is investigated via ultrafast transient absorption spectroscopy (TAS) and time-resolved photoluminescence (TRPL). The photoexcited carrier first injected to the ZnS shell in 2 ps, then relaxed to alloyed layer between the ZnS shell and InP core in 7.4 ps, and next relaxed to different energy levels in the InP core in about 180 ps. After relaxation or cooling, the charged excitons and neutral excitons recombined in 4.1 and 26.7 ns. In addition, the intrinsic TPA of InP/ZnS QDs was investigated; the corresponding σ_2 are inferred to be 4.26×10^{-47} cm^4 s photon^{-1} (or 3.5×10^3 GM), which indicates good nonlinear optical properties. Time constants (durations) for different optoelectronic processes occurred in the composite QDs. On the basis of these time constants of the primary exciton dynamics, it is significant for the improvement and engineering InP/ZnS QDs based materials in optoelectronic applications.

■ ASSOCIATED CONTENT

Supporting Information

The Supporting Information is available free of charge on the ACS Publications website at DOI: 10.1021/acs.jpcc.9b07092.

Raman spectra of InP/ZnS QDs; normal TEM images of InP QDs and InP/ZnS QDs; transient absorption spectra of InP/ZnS QDs at the wavelength before 400 nm (PDF)

■ AUTHOR INFORMATION

Corresponding Authors

*E-mail: wxw4122@cust.edu.cn (X.W.).
*E-mail: biewang2001@126.com (X.W.).
*E-mail: chenr@sustech.edu.cn (R.C.).

ORCID

Xuan Fang: 0000-0003-2290-4951
Xiaohua Wang: 0000-0002-6984-1970
Rui Chen: 0000-0002-0445-7847

Author Contributions

The manuscript was written through contributions of all authors. All authors have given approval to the final version of the manuscript. X.H.W. and R.C. conceived and designed the experiments. Both authors performed the experiments, analyzed the data, and wrote the manuscript.

Notes

The authors declare no competing financial interest.

■ ACKNOWLEDGMENTS

This work was supported by the National Natural Science Foundation of China (11674038, 61674021, and 61704011), the Foundation of State Key Laboratory of High Power Semiconductor Lasers, the Innovation Foundation of Changchun University of Science and Technology (XJJLG-2016-11 and XJJLG-2016-14), and the Foundation of NANO X (18JG01). R.C. was supported by the National Natural Science Foundation of China (11574130) and the Shenzhen Science and Technology Innovation Commission (Projects KQJSCX20170726145748464, JCYJ20180305180553701, and KQTD2015071710313656).

■ ABBREVIATIONS

QDs, quantum dots; PL, photoluminescence; QY, quantum yield; XRD, X-ray diffraction; TEM, transmission electron microscopy; TAS, transient absorption spectroscopy; TRPL, time-resolved photoluminescence; TPA, two-photon absorption.

■ REFERENCES

(1) Bao, J.; Bawendi, M. G. A Colloidal Quantum Dot Spectrometer. *Nature* **2015**, *523*, 67−70.
(2) Bourzac, K. Quantum Dots Go on Display. *Nature* **2013**, *493*, 283.
(3) Bruchez, M., Jr.; et al. Semiconductor Nanocrystals as Fluorescent Biological Labels. *Science* **1998**, *281*, 2013−2016.
(4) Sun, Q.; Wang, Y. A.; Li, L. S.; Wang, D.; Zhu, T.; Xu, J.; Yang, C.; Li, Y. Bright, Multicoloured Light-Emitting Diodes Based on Quantum Dots. *Nat. Photonics* **2007**, *1*, 717−722.
(5) Klimov, V. I.; Mikhailovsky, A. A.; Xu, S.; Malko, A.; Hollingsworth, J. A.; Leatherdale, C. A.; Eisler, H.; Bawendi, M. G. Optical Gain and Stimulated Emission in Nanocrystal Quantum Dots. *Science* **2000**, *290*, 314−317.
(6) Lorenzon, M.; Christodoulou, S.; Vaccaro, G.; Pedrini, J.; Meinardi, F.; Moreels, I.; Brovelli, S. Reversed Oxygen Sensing Using Colloidal Quantum Wells Towards Highly Emissive Photoresponsive Varnishes. *Nat. Commun.* **2015**, *6*, 6434.
(7) Nozik, A. J. Quantum Dot Solar Cells. *Phys. E (Amsterdam, Neth.)* **2002**, *14*, 115−120.
(8) Tamang, S.; Lincheneau, C.; Hermans, Y.; Jeong, S.; Reiss, P. Chemistry of InP Nanocrystal Syntheses. *Chem. Mater.* **2016**, *28*, 2491−2506.
(9) Mushonga, P.; Onani, M. O.; Madiehe, A. M.; Meyer, M. Indium Phosphide-Based Semiconductor Nanocrystals and Their Applications. *J. Nanomater.* **2012**, *2012*, 869284.
(10) Reiss, P.; Protière, M.; Li, L. Core/Shell Semiconductor Nanocrystals. *Small* **2009**, *5*, 154−168.
(11) Vasudevan, D.; Gaddam, R. R.; Trinchi, A.; Cole, I. S. Core-Shell Quantum Dots: Properties and Applications. *J. Alloys Compd.* **2015**, *636*, 395−404.
(12) Micic, O. I.; Sprague, J.; Lu, Z.; Nozik, A. J. Highly Efficient Band-Edge Emission from InP Quantum Dots. *Appl. Phys. Lett.* **1996**, *68*, 3150−3152.
(13) Micic, O. I.; Ahrenkiel, S. P.; Nozik, A. J. Synthesis of Extremely Small InP Quantum Dots and Electronic Coupling in Their Disordered Solid Films. *Appl. Phys. Lett.* **2001**, *78*, 4022.
(14) Micic, O. I.; Smith, B. B.; Nozik, A. J. Core−Shell Quantum Dots of Lattice-Matched $ZnCdSe_2$ Shells on InP Cores: Experiment and Theory. *J. Phys. Chem. B* **2000**, *104*, 12149−12156.
(15) Micic, O. I.; Curtis, C. J.; Jones, K. M.; Sprague, J. R.; Nozik, A. J. Synthesis and Characterization of InP Quantum Dots. *J. Phys. Chem.* **1994**, *98*, 4966−4969.
(16) Battaglia, D.; Peng, X. Formation of High Quality InP and InAs Nanocrystals in a Noncoordinating Solvent. *Nano Lett.* **2002**, *2*, 1027−1030.
(17) Xie, R.; Battaglia, D.; Peng, X. Colloidal InP Nanocrystals as Efficient Emitters Covering Blue to near-Infrared. *J. Am. Chem. Soc.* **2007**, *129*, 15432−15433.
(18) Lee, J. C.; Jang, E.-P.; Jang, D. S.; Choi, Y.; Choi, M.; Yang, H. Solvothermal Preparation and Fluorescent Properties of Color-Tunable InP/ZnS Quantum Dots. *J. Lumin.* **2013**, *134*, 798−805.
(19) Tamang, S.; Lincheneau, C.; Hermans, Y.; Jeong, S.; Reiss, P. Chemistry of InP Nanocrystal Syntheses. *Chem. Mater.* **2016**, *28*, 2491−2506.
(20) Pham, T. T.; Chi Tran, T. K.; Nguyen, Q. L. Temperature-Dependent Photoluminescence Study of InP/ZnS Quantum Dots. *Adv. Nat. Sci.: Nanosci. Nanotechnol.* **2011**, *2*, 025001.

DOI: 10.1021/acs.jpcc.9b07092
J. Phys. Chem. C 2019, 123, 27207−27213

(21) Narayanaswamy, A.; Feiner, L. F.; van der Zaag, P. J. Temperature Dependence of the Photoluminescence of InP/ZnS Quantum Dots. *J. Phys. Chem. C* **2008**, *112*, 6775−6780.
(22) Narayanaswamy, A.; Feiner, L. F.; Meijerink, A.; van der Zaag, P. J. The Effect of Temperature and Dot Size on the Spectral Properties of Colloidal InP/ZnS Core-Shell Quantum Dots. *ACS Nano* **2009**, *3*, 2539−2546.
(23) Biadala, L.; Siebers, B.; Beyazit, Y.; Tessier, M. D.; Dupont, D.; Hens, Z.; Yakovlev, D. R.; Bayer, M. Band-Edge Exciton Fine Structure and Recombination Dynamics in InP/ZnS Colloidal Nanocrystals. *ACS Nano* **2016**, *10*, 3356−3364.
(24) Thuy, P. T.; Thuy, U. T. D.; Chi, T. T. K.; Phuong, L. Q.; Liem, N. Q.; Li, L.; Reiss, P. Time-Resolved Photoluminescence Measurements of InP/ZnS Quantum Dots. *J. Phys.: Conf. Ser.* **2009**, *187*, 012014.
(25) Sheikbahae, M.; Said, A. A.; Wei, T.; Hagan, D. J.; Van Stryland, E. W. Sensitive Measurement of Optical Nonlinearities Using a Single Beam. *IEEE J. Quantum Electron.* **1990**, *26*, 760−769.
(26) Peng, X.; Schlamp, M. C.; Kadavanich, V. A.; Alivisatos, A. P. Epitaxial Growth of Highly Luminescent CdSe/CdS Core/Shell Nanocrystals with Photostability and Electronic Accessibility. *J. Am. Chem. Soc.* **1997**, *119*, 7019−7029.
(27) Li, L.; Reiss, P. One-Pot Synthesis of Highly Luminescent InP/ZnS Nanocrystals without Precursor Injection. *J. Am. Chem. Soc.* **2008**, *130*, 11588−11589.
(28) Xu, S.; Ziegler, J.; Nann, T. Rapid Synthesis of Highly Luminescent InP and InP/ZnS Nanocrystals. *J. Mater. Chem.* **2008**, *18*, 2653−2656.
(29) Tessier, M. D.; Dupont, D.; De Nolf, K.; De Roo, J.; Hens, Z. Economic and Size-Tunable Synthesis of InP/ZnE (E = S,Se) Colloidal Quantum Dots. *Chem. Mater.* **2015**, *27*, 4893−4898.
(30) Ning, J.; Zheng, C.; Zhang, X.; Xu, S. Strong Quantum Confinement Effect and Reduced Frohlich Exciton-Phonon Coupling in ZnO Quantum Dots Embedded inside a SiO_2 Matrix. *Nanoscale* **2015**, *7*, 17482−17487.
(31) Bae, W. K.; Padilha, L. A.; Park, Y.-S.; McDaniel, H.; Robel, I.; Pietryga, J. M.; Klimov, V. I. Controlled Alloying of the Core−Shell Interface in CdSe/CdS Quantum Dots for Suppression of Auger Recombination. *ACS Nano* **2013**, *7*, 3411−3419.
(32) Park, Y.-S.; Bae, W. K.; Baker, T.; Lim, J.; Klimov, V. I. Effect of Auger Recombination on Lasing in Heterostructured Quantum Dots with Engineered Core/Shell Interfaces. *Nano Lett.* **2015**, *15*, 7319−7328.
(33) Matylitsky, V. V.; Dworak, L.; Breus, V. V.; Basché, T.; Wachtveitl, J. Ultrafast Charge Separation in Multiexcited CdSe Quantum Dots Mediated by Adsorbed Electron Acceptors. *J. Am. Chem. Soc.* **2009**, *131*, 2424−2425.
(34) Zhu, H.; Song, N.; Lian, T. Controlling Charge Separation and Recombination Rates in CdSe/ZnS Type I Core-Shell Quantum Dots by Shell Thicknesses. *J. Am. Chem. Soc.* **2010**, *132*, 15038−15045.
(35) Wojdyla, M.; Gallagher, S. A.; Moloney, M. P.; Gun'Ko, Y. K.; Kelly, J. M.; Magno, L. M.; Quinn, S. J.; Clark, I. P.; Greetham, G. M.; Towrie, M. Picosecond to Millisecond Transient Absorption Spectroscopy of Broad-Band Emitting Chiral CdSe Quantum Dots. *J. Phys. Chem. C* **2012**, *116*, 16226−16232.
(36) Wang, Y. F.; Wang, H. Y.; Li, Z. S.; Zhao, J.; Wang, L.; Chen, Q. D.; Wang, W. Q.; Sun, H. B. Electron Extraction Dynamics in Cdse and CdSe/CdS/ZnS Quantum Dots Adsorbed with Methyl Viologen. *J. Phys. Chem. C* **2014**, *118*, 17240−17246.
(37) Busby, E.; Thibert, A.; Fuzell, J.; Arrington, D. C.; Jawaid, A. M.; Snee, P. T.; Larsen, D. S. Ultrafast Exciton Dynamics in Colloidal Aluminum Phosphide Nanocrystals. *Chem. Phys. Lett.* **2013**, *557*, 129−133.
(38) Reid, K. R.; Mcbride, J. R.; Freymeyer, N. J.; Thal, L. B.; Rosenthal, S. J. Chemical Structure, Ensemble and Single-Particle Spectroscopy of Thick-Shell InP-ZnSe Quantum Dots. *Nano Lett.* **2018**, *18*, 709−716.
(39) Zheng, C. C.; Xu, S. J.; Ning, J. Q.; Chen, Y. N.; Li, B. K.; Wang, J. N.; Che, C. M. Formation Dynamics of Excitons and Temporal Behaviors of Fano Resonance Due to the Exciton-Impurity-Phonon Configuration Interaction in ZnO. *J. Phys. Chem. A* **2012**, *116*, 381−385.
(40) Comanescu, G.; Wang, W. B.; Gundry, S.; Das, B.; Alfano, R. R.; Perez-Paz, M. N.; Tamargo, M. C.; Munoz, M.; Popov, I.; Isaacs, L. L. Spectroscopy and Carrier Dynamics in Cdse Self-Assembled Quantum Dots Embedded in $Zn_xCd_yMg_{1-x-y}Se$. *Appl. Phys. Lett.* **2005**, *86*, 253113.
(41) Kundys, D. O.; Murzyn, P.; Wells, J.-P. R.; Tartakovskii, A. I.; Skolnick, M. S.; Dang, L. S.; Lutsenko, E. V.; Tarasuk, N. P.; Lyublinskaya, O. G.; Toropov, A. A.; Ivanov, S. V. The Dynamics of Amplified Spontaneous Emission in CdSe/ZnSe Quantum Dots. *J. Appl. Phys. (Melville, NY, U. S.)* **2006**, *100*, 123510.
(42) Bae, W. K.; Park, Y.-S.; Lim, J.; Lee, D.; Padilha, L. A.; McDaniel, H.; Robel, I.; Lee, C.; Pietryga, J. M.; Klimov, V. I. Controlling the Influence of Auger Recombination on the Performance of Quantum-Dot Light-Emitting Diodes. *Nat. Commun.* **2013**, *4*, 2661.
(43) Wang, Y.; Yang, X.; He, T. C.; Gao, Y.; Demir, H. V.; Sun, X. W.; Sun, H. D. Near Resonant and Nonresonant Third-Order Optical Nonlinearities of Colloidal InP/ZnS Quantum Dots. *Appl. Phys. Lett.* **2013**, *102*, 021917.
(44) Joly, A. G.; Chen, W.; McCready, D. E.; Malm, J.-O.; Bovin, J.-O. Upconversion Luminescence of CdTe Nanoparticles. *Phys. Rev. B: Condens. Matter Mater. Phys.* **2005**, *71*, 165304.
(45) Reiss, P.; Protiere, M.; Li, L. Core/Shell Semiconductor Nanocrystals. *Small* **2009**, *5*, 154−168.
(46) Li, X.; Van Embden, J.; Chon, J. W. M.; Gu, M. Enhanced Two-Photon Absorption of CdS Nanocrystal Rods. *Appl. Phys. Lett.* **2009**, *94*, 103117.
(47) Pan, L.; Tamai, N.; Kamada, K.; Deki, S. Nonlinear Optical Properties of Thiol-Capped CdTe Quantum Dots in Nonresonant Region. *Appl. Phys. Lett.* **2007**, *91*, 051902.
(48) Zhu, B. H.; Zhang, H.; Zhang, J.; Cui, Y.; Zhou, Z. Surface-Related Two-Photon Absorption and Refraction of CdSe Quantum Dots. *Appl. Phys. Lett.* **2011**, *99*, 021908.

DOI: 10.1021/acs.jpcc.9b07092
J. Phys. Chem. C 2019, 123, 27207−27213